

A Transition in the Pairing Symmetry of the Electron-Doped Cuprates

John A. Skinta and Thomas R. Lemberger

Department of Physics, Ohio State University, Columbus, OH 43210-1106

T. Greibe and M. Naito

NTT Basic Research Laboratories, 3-1 Morinosato Wakamiya, Atsugi-shi, Kanagawa 243, Japan

(December 2, 2024)

We present measurements of the penetration depth, $\lambda^{-2}(T)$, in $\text{Pr}_{2-x}\text{Ce}_x\text{CuO}_4$ and $\text{La}_{2-x}\text{Ce}_x\text{CuO}_4$ films at three doping levels, x , near optimal. Optimal and overdoped films are qualitatively and quantitatively different from underdoped films, e.g., $\lambda^{-2}(0)$ is twice as large and $\lambda^{-2}(T)$ is cubic rather than quadratic at low T . We propose that these differences signal a transition from d - to s -wave pairing near optimal doping.

PACS numbers: 74.25.Fy, 74.76.Bz, 74.72.Jt

A variety of experiments have demonstrated that hole-doped cuprates possess a predominantly $d_{x^2-y^2}$ gap [1,2]. In contrast, there is no consensus concerning order parameter symmetry in electron-doped cuprates. Phase-sensitive [3], ARPES [4], and some penetration depth [5,6] measurements on optimally doped $\text{Pr}_{2-x}\text{Ce}_x\text{CuO}_4$ (PCCO) and $\text{Nd}_{2-x}\text{Ce}_x\text{CuO}_4$ (NCCO) samples suggest d -wave pairing. Other penetration depth measurements [7,8] and the absence of a zero-bias conductance peak in tunnelling measurements [9,10] indicate s -wave superconductivity.

To date, experimental studies of e-doped cuprates have concentrated on optimally doped samples. To explore the doping dependence of e-doped cuprate properties and to resolve the pairing symmetry controversy, we present measurements of $\lambda^{-2}(T)$ in PCCO and $\text{La}_{2-x}\text{Ce}_x\text{CuO}_4$ (LCCO) thin films at three dopings, x , near optimal. The curvature near T_c and the low- T magnitude of the superfluid density, $n_s(T) \propto \lambda^{-2}(T)$, depend strongly on doping. Furthermore, the T -dependence of $\lambda^{-2}(T)/\lambda^{-2}(0)$ at low T changes with doping: it is cubic at optimal and overdoping, but quadratic at underdoping. These phenomena indicate some sort of transition near optimal doping. We propose that the transition is from d - to s -wave pairing. Contradictory e-doped pairing symmetry results can thus be reconciled, if nominally optimally doped samples that exhibit d -wave properties are in reality underdoped.

Films were prepared by molecular-beam epitaxy (MBE) on $12.7 \text{ mm} \times 12.7 \text{ mm} \times 0.35 \text{ mm}$ SrTiO_3 substrates as detailed elsewhere [11–13]. Table I summarizes important film parameters. Ce concentrations are measured by inductively coupled plasma spectroscopy and are known to better than ± 0.005 . We refer to the LCCO film with $x = 0.112$ and the PCCO film with $x = 0.145$ as “optimally doped”, although on the basis of data presented below, we estimate that optimal x is actually slightly smaller than these values. The optimal PCCO film is film P2 from Ref. 8. The films are highly c -axis oriented, and their ab -plane resistivities, $\rho(T)$ (Fig. 1), are low. $\rho(T)$ decreases monotonically with increasing doping. $\rho(T)$ just above T_c decreases by a factor of two between under- and optimally doped films.

We measure $\lambda^{-2}(T)$ with a two-coil mutual inductance technique described in detail elsewhere [14]. Films are centered between two coils each approximately 2 mm in diameter and 1 mm long. The sample is cooled to 1.6 K, and a current of $\leq 10 \text{ mA}$ is driven at 50 kHz through the drive coil. As T slowly increases, the voltage induced in the pickup coil is measured continuously. Measurements are made at several drive currents to ensure that data are taken in the linear response regime. The current density induced in the film is essentially uniform through its thickness. Because the coils are much smaller than the film, the applied field is concentrated near the center of the film and demagnetizing effects at the edges are irrelevant.

The film’s sheet conductivity, $\sigma(T)d = \sigma_1(T)d - i\sigma_2(T)d$ with d the film thickness, is deduced from the measured mutual inductance. σ_1 is large enough to be detectable only near T_c . We define T_c and ΔT_c to be the temperature and full width of the peak in σ_1 . $\lambda^{-2}(T)$ is obtained from the imaginary part of the conductivity as $\lambda^{-2}(T) \equiv \mu_0\omega\sigma_2(T)$, where μ_0 is the magnetic permeability of vacuum. Experimental noise, about 0.2% of $\lambda^{-2}(0)$, is limited by amplifier drift. 15% uncertainty in d is the largest source of error in $\lambda^{-2}(T)$. This uncertainty does not impact the T -dependence of $\lambda^{-2}(T)/\lambda^{-2}(0)$. As the films were grown in the same MBE apparatus on successive runs, we estimate the relative uncertainty in $\lambda^{-2}(0)$ in each material to be $\sim 10\%$.

Measurement of $\sigma_1(T)$ is a stringent test of film quality, as inhomogeneities in any layer will increase ΔT_c . Figure 2 displays $\sigma_1(T)$ measured at 50 kHz for each film. ΔT_c is typically $\leq 1 \text{ K}$, indicating excellent film quality. Multiple peaks in σ_1 indicate layers with slightly different T_c ’s. The small peak at 19.7 K in the overdoped LCCO data is probably due to a tiny bad spot at the film edge. No corresponding feature in $\lambda^{-2}(T)$ is apparent at 19.7 K (Fig. 3),

indicating that this transition is unimportant to analysis of the data.

A few more words about film quality are in order. Maximum T_c 's of e-doped films [7,8,10] are the same as or superior to those of crystals [4–6,15]. Resistivities of films are lower [15,16]. Crystals have intrinsic homogeneity problems, i.e., Ce-poor surfaces and gradients in Ce content [17,18]. The reduction process required to remove interstitial apical oxygen causes phase decomposition in bulk samples [11]. Optimized LCCO crystals have yet to be grown, so we cannot compare LCCO films with crystals [13].

Figure 3 displays $\lambda^{-2}(T)$ for all films. Evolution of $\lambda^{-2}(T)$ with doping is the same in PCCO and LCCO, although the optimal T_c of LCCO is 20% higher than PCCO. Quantitatively, $\lambda^{-2}(0)$ is about the same at optimal and overdoping, but is a factor of 2 smaller at underdoping. Qualitatively, puzzling upward curvature in $\lambda^{-2}(T)$ near T_c develops abruptly at optimal doping and grows with overdoping. We emphasize that the upward curvature seen in these films is *not* due to inhomogeneity, as the feature extends far below the sharp peak in σ_1 [19].

We now examine the low- T behavior of $\lambda^{-2}(T)$, Fig. 4 and Fig. 5. We have previously found that $\lambda^{-2}(T)$ in five optimal PCCO films is reproducibly cubic at low T :

$$\lambda^{-2}(T) \sim \lambda^{-2}(0) \left[1 - \left(\frac{T}{T_0} \right)^3 \right], \quad (1)$$

with the same coefficient, $T_0 = 20 \pm 1$ K [8]. In optimal LCCO (Fig. 5), $(T/T_0)^3$ fits the first 5% drop in $\lambda^{-2}(T)$ within experimental noise, with a value of $T_0 = 21.8$ K, that is essentially the same as for optimal PCCO. A quadratic fit lies outside experimental noise. In overdoped PCCO and LCCO (Fig. 4), the first 8% drop in $\lambda^{-2}(T)/\lambda^{-2}(0)$ is well fitted by $(T/T_0)^3$, with values of T_0 (13.3 K and 9.0 K, respectively) substantially smaller than at optimal doping. The best quadratic fit, $(T/T_0)^2$, to PCCO lies well outside experimental noise in places and is unacceptable. For LCCO, the case is less clear; data at lower T are needed to eliminate T^2 definitively.

In underdoped PCCO and LCCO (Fig. 5), a quadratic fit, $(T/T_0)^2$, to the first 7 to 9% drop in $\lambda^{-2}(T)/\lambda^{-2}(0)$ is better than cubic. For PCCO, the distinction is clear, while for LCCO it is less clear. Values of T_0 from quadratic fits are quite different, 38.6 K and 20.0 K for LCCO and PCCO, respectively.

The picture that emerges from the data is that there is some sort of transition near optimal doping. Three different features of the superfluid density change abruptly. In our PCCO films, the changes occur at essentially the same T_c . We note that there is an abrupt transition in the behavior of h-doped cuprates near optimal doping, which is associated with the onset of a pseudogap [20]. It may be coincidental that there are transitions in e-doped and h-doped cuprate behavior near optimal doping.

We can only speculate as to the nature of the transition. On the basis of the low- T transition from quadratic to cubic behavior, we surmise that pairing changes from d -wave to s -wave. There exists a model for s -wave superconductors in which cubic behavior occurs, i.e., due to inelastic electron-phonon scattering [21], but there is no such d -wave model. d -wave models predict quadratic behavior at low T [22–24]. This issue was discussed in more detail in Ref. 8.

The enhancement of upward curvature in $\lambda^{-2}(T)$ near T_c with increased doping is puzzling. $\lambda^{-2}(T)$ has downward curvature or is linear near T_c at underdoping, while upward curvature develops at optimal and overdoping. Mean-field theories typically predict downward curvature. Thermal fluctuations only make downward curvature stronger as T approaches T_c from below. We reemphasize that upward curvature is *not* associated with a spread in T_c 's in the films.

We have presented measurements of $\lambda^{-2}(T)$ from 1.6 K through T_c in PCCO and LCCO films at various dopings near optimal. Film quality is demonstrably high, and PCCO and LCCO behave similarly with doping. $\lambda^{-2}(0)$ is the same at optimal and overdoping but decreases by a factor of 2 at underdoping. Upward curvature in $\lambda^{-2}(T)$ near T_c develops at optimal doping and grows with overdoping. At low T , $\lambda^{-2}(T)$ is cubic at optimal and overdoping, and is quadratic at underdoping. T^3 behavior is consistent with an s -wave order parameter with strong inelastic scattering, while T^2 indicates d -wave superconductivity. This apparent transition in pairing symmetry reconciles contradictory literature results on e-doped cuprates, if nominally optimally doped samples that exhibit d -wave characteristics are in reality underdoped.

This work was supported in part by DoE Grant DE-FG02-90ER45427 through the Midwest Superconductivity Consortium.

[1] D.J. Van Harlingen, Rev. Mod. Phys. **67**, 515 (1995).

- [2] C.C. Tsuei and J.R. Kirtley, Rev. Mod. Phys. **72**, 969 (2000).
- [3] C.C. Tsuei and J.R. Kirtley, Phys. Rev. Lett. **85**, 182 (2000).
- [4] N.P. Armitage *et al.*, Phys. Rev. Lett. **86**, 1126 (2001).
- [5] J.D. Kokales *et al.*, Phys. Rev. Lett. **85**, 3696 (2000).
- [6] R. Prozorov *et al.*, Phys. Rev. Lett. **85**, 3700 (2000).
- [7] L. Alff *et al.*, Phys. Rev. Lett. **83**, 2644 (1999).
- [8] J.A. Skinta *et al.*, submitted to Phys. Rev. Lett.
- [9] S. Kashiwaya *et al.*, Phys. Rev. B **57**, 8680 (1998).
- [10] L. Alff *et al.*, Phys. Rev. B **58**, 11197 (1998).
- [11] M. Naito *et al.*, Physica (Amsterdam) **293C**, 36 (1997).
- [12] M. Naito and H. Sato, Appl. Phys. Lett. **67**, 2557 (1995); H. Yamamoto *et al.*, Phys. Rev. B **56**, 2852 (1997).
- [13] M. Naito and M. Hepp, Jpn. J. Appl. Phys. Lett. **39**, 485 (2000).
- [14] S.J. Turneaure *et al.*, J. Appl. Phys. **79**, 4221 (1996); S.J. Turneaure *et al.*, *ibid.* **83**, 4334 (1998).
- [15] J.D. Kokales *et al.*, Physica (Amsterdam) **341-348C**, 1655 (2000).
- [16] P. Fournier *et al.*, Phys. Rev. Lett. **81**, 4720 (1998).
- [17] A.R. Drews *et al.*, Physica (Amsterdam) **200C**, 122 (1992).
- [18] E.F. Skelton *et al.*, Science **263**, 1416 (1994).
- [19] We have observed upward curvature in λ^{-2} near T_c before, but never at T below the fluctuation peak in σ_1 . We ascribe upward curvature with non-zero σ_1 to film inhomogeneity.
- [20] T. Timusk and B. Statt, Rep. Prog. Phys. **62**, 61 (1999).
- [21] G.V. Klimovich *et al.*, JETP Lett. **53**, 399 (1991).
- [22] J.F. Annett *et al.*, in *Physical Properties of High Temperature Superconductors II*, edited by D.M. Ginsberg (World Scientific, Singapore, 1990).
- [23] P.J. Herschfeld and N. Goldenfeld, Phys. Rev. B **48**, 4219 (1993).
- [24] I. Kosztin and A.J. Leggett, Phys. Rev. Lett. **79**, 135 (1997).

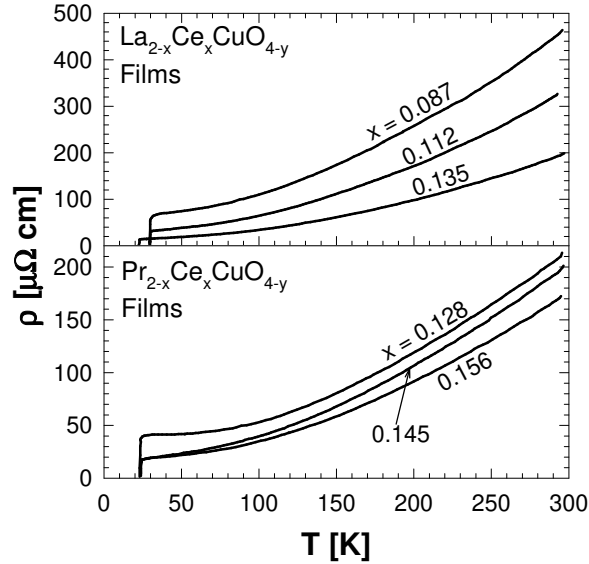


FIG. 1. *ab*-plane resistivities, $\rho(T)$, of six electron-doped films. For resistivities just above T_c , see Table I.

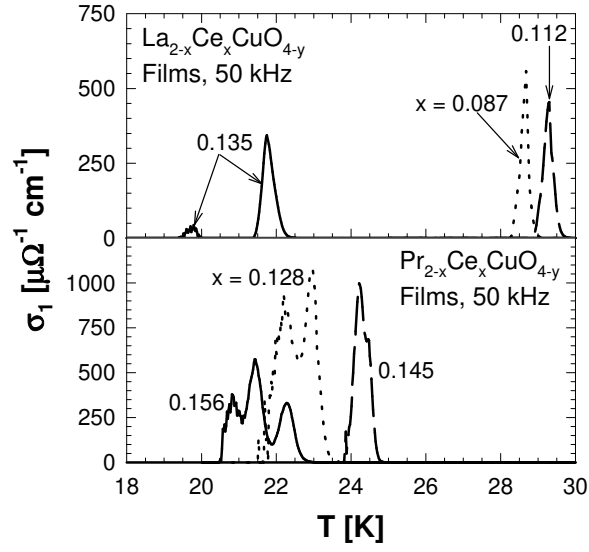


FIG. 2. $\sigma_1(T)$ at 50 kHz in six electron-doped films. T_c and ΔT_c are temperature and full width of peak in σ_1 .

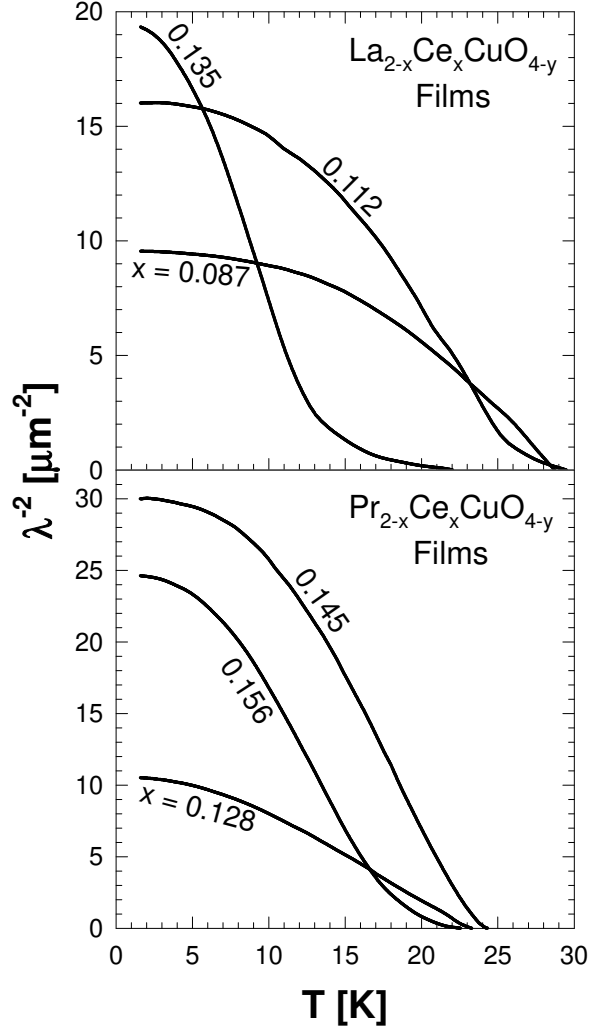


FIG. 3. $\lambda^{-2}(T)$ in six electron-doped films. Relative uncertainty in $\lambda^{-2}(0)$ in each material is $\sim 10\%$.

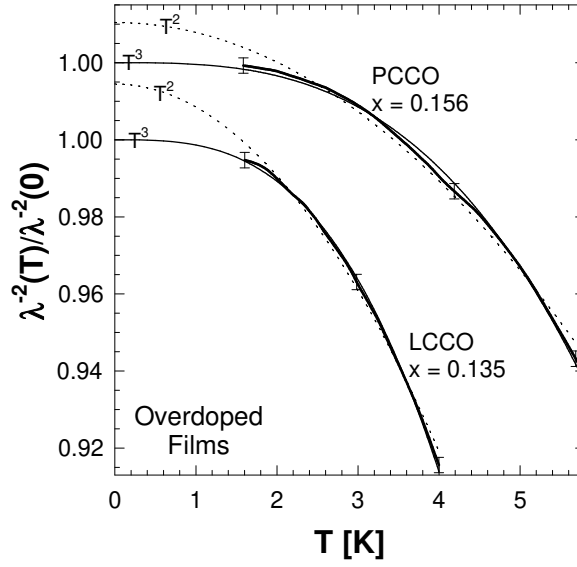


FIG. 4. First 8% drop in $\lambda^{-2}(T)/\lambda^{-2}(0)$ for overdoped PCCO and LCCO films (thick lines), offset for clarity. Error bars represent experimental noise of 0.2%. Thin solid (dotted) lines are best cubic (quadratic) fits to $\lambda^{-2}(T)/\lambda^{-2}(0)$ over this range. Cubic fits are superior.

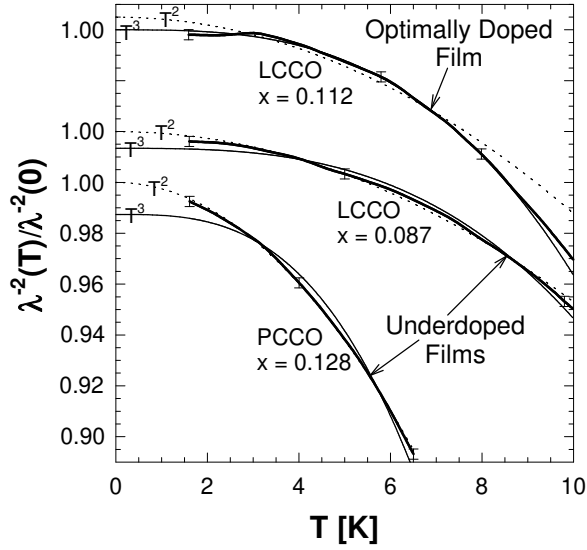


FIG. 5. $\lambda^{-2}(T)/\lambda^{-2}(0)$ at low T for optimal (upper curve) and underdoped (lower curves) electron-doped films, offset for clarity. Error bars represent experimental noise of 0.2%. Thin solid (dotted) lines are best cubic (quadratic) fits to $\lambda^{-2}(T)/\lambda^{-2}(0)$ over this range. For optimal LCCO, the fit extends only to 8 K and is extrapolated to higher T . The optimal film is cubic, and the underdoped films quadratic, at low T .

TABLE I. Properties of six electron-doped films. Ce doping, x , is measured by inductively coupled plasma spectroscopy to better than ± 0.005 . d is nominal film thickness. T_c and ΔT_c are location and full width of peak in σ_1 . T_0 is determined from best cubic (optimal and overdoped films) and quadratic (underdoped films) fits to first 8% drop in $\lambda^{-2}(T)$. Absolute uncertainty in $\lambda^{-2}(0)$ is $\pm 15\%$.

Film	x	d [Å]	T_c [K]	ΔT_c [K]	T_0 [K]	$\lambda(0)$ [Å]	$\rho(T_c + 5K)$ [$\mu\Omega\text{cm}$]
underdoped LCCO	0.087	1250	28.7	0.8	38.6	3200	70
optimal LCCO	0.112	1250	29.3	0.9	21.8	2500	35
overdoped LCCO	0.135	1250	21.7	1.0	9.0	2300	20
underdoped PCCO	0.128	1000	22.5	1.8	20.0	3100	40
optimal PCCO	0.145	1000	24.2	1.0	19.1	1800	20
overdoped PCCO	0.156	1000	21.5	2.4	13.3	2000	20